2D Materials

Confocal laser scanning microscopy as a real-time quality-assessment tool for industrial graphene synthesis

2D Materials

PAPER

Confocal laser scanning microscopy as a real-time quality-assessment tool for industrial graphene synthesis

Dong Jin Kim[1,2,4,9], **Chang-Won Lee**[5,9], **Yeonjoon Suh**[2,3], **Heejeong Jeong**[6], **Insu Jo**[2,3], **Joonhee Moon**[7], **Mina Park**[2,3], **Yun Sung Woo**[4,8] and **Byung Hee Hong**[2,3,4]

[1] Program in Nano Science and Technology, Graduate School of Convergence Science and Technology, Seoul National University, Seoul 08826, Republic of Korea
[2] Graphene Research Center, Advanced Institute of Convergence Technology, Suwon 16229, Republic of Korea
[3] Department of Chemistry, Seoul National University, Seoul 08826, Republic of Korea
[4] Graphene Square Inc., Suwon 16229, Republic of Korea
[5] Faculty of Science, Institute of Advanced Optics and Photonics, Department of Applied Optics, School of Basic Sciences, Hanbat National University, Daejeon 34158, Republic of Korea
[6] Department of Physics, University of Malaya, Kuala Lumpur 50603, Malaysia
[7] Research Center for Materials Analysis, Korea Basic Science Institute, Daejeon 34133, Republic of Korea
[8] Department of Materials Science and Engineering, Dankook University, Chungnam 31116, Republic of Korea

E-mail: byunghee@snu.ac.kr **and** yunswoo@dankook.ac.kr

Keywords: graphene, CLSM, real-time quality-assessment, optical conductivity

Supplementary material for this article is available online

OPEN ACCESS

RECEIVED
30 March 2020

REVISED
12 June 2020

ACCEPTED FOR PUBLICATION
1 July 2020

PUBLISHED
27 July 2020

Abstract

For the industrial quality control (QC) of the chemical vapor deposition (CVD) graphene, it is essential to develop a method to screen out unsatisfactory graphene films as efficiently as possible. However, previously proposed methods based on Raman spectroscopy or optical imaging after chemical etching are unable to provide non-invasive and fast analysis of large-area graphene films as grown on Cu foil substrates. Here we report that the reflection mode of confocal laser scanning microscopy (CLSM) provides a high-contrast image of graphene on Cu, enabling the real-time evaluation of the coverage and quality of graphene. The reflectance contrast, *Rc*, was found to be dependent on the incident laser wavelength, of which the maximum was obtained at 405 nm. In addition, *Rc* decreases with increasing defect density of graphene. The dependence of *Rc* on the graphene's quality and laser wavelengths were explained by the tight-binding model calculation based on the Fresnel's interference formula. Thus, we believe that the reflection mode CLSM would be a very powerful quality-assessment tool for the mass production of CVD graphene films grown on Cu.

1. Introduction

Large-area, high-quality, and continuous growth technologies for CVD graphene have been developed to meet the requirements for industrial applications [1–3]. However, there has been a lack of proper methods to check the quality of graphene in a rapid yet non-destructive way for a mass-production scale [4–6]. Optical microscopy (OM) has been widely explored for imaging and characterizing CVD graphene directly on Cu [7–13]. Dark field (DF) OM was employed to investigate CVD graphene grown on Cu foil using the Rayleigh light scattering from Cu steps beneath graphene, which can be adopted only for metals that generate steps with considerable height differences [9]. Moreover, DF imaging by weak scattered light is time-consuming and requires a sample of graphene on Cu foil to be placed under illumination for an extended period time. Thus, we propose the reflection mode of confocal laser scanning microscopy (CLSM) as a real-time evaluation tool to monitor the coverage and quality of graphene, as CLSM is capable of scanning a large area within a few seconds in high-resolution, which is expected to enable faster characterization of graphene as grown on Cu regardless of its production scale.

The reflection mode CLSM possesses a great potential to be utilized for the *in-situ* monitoring

[9] These authors contributed equally.

of the CVD-grown graphene on Cu foil as a quality assessment tool of mass-produced CVD graphene films [14–16]. The CLSM generates high-contrast optical images of CVD-grown graphene on Cu over a large area with higher contrast between the graphene layer and Cu for shorter incident laser wavelengths. Furthermore, the quality of CVD graphene can be characterized by CLSM because the reflectance and the optical conductivity are inversely proportional to the defect density [17], rendering it a quality assessment tool of mass-produced CVD graphene particularly important for roll-to-roll (R2R) processes (see supplementary figure S1 (available online at stacks.iop.org/2DM/7/045014/mmedia) for the indication of the quality assessment step during full R2R processes).

2. Results

2.1. Highly visible CLSM image of CVD graphene on Cu foil

Figure 1(a) illustrates the concept of monitoring the as-grown CVD graphene on Cu foil throughout the continuous roll-to-roll synthetic process using the reflective mode CLSM. In this experiment, the CVD graphene with various coverage from sub-monolayer to fully covered was grown on Cu foil by controlling the growth time. As shown in figures 1(b) and (c), the reflection mode CLSM image of CVD-grown graphene on Cu foil precisely reveals the coverage of graphene on Cu foil; graphene is observed as a bright region while Cu is observed as a dark region. For sub-monolayer graphene samples with coverage less than 100%, graphene is precisely distinguishable from Cu due to the high contrast between graphene and Cu, which makes it easy to identify areas where the graphene is not covered. Meanwhile, the fully covered graphene samples did not show any contrast in CLSM image as shown in figure 1(d). In practice, the CLSM that provides high visibility of graphene on Cu can be used as a powerful tool to monitor whether graphene on Cu foil is fully grown, which is indispensable for quality assessment of CVD graphene in a mass synthetic process.

Figures 2(a)–(c) compare the images of CVD-grown graphene on Cu foil using conventional bright field (BF), dark field (DF) microscopy, and CLSM in the same region. It reveals that the reflection mode CLSM offers a significant improvement over BF and DF for imaging graphene on Cu. It is well known that Cu is immediately oxidized in air, turning dark yellow in the BF, which allows the faint distinction between graphene and Cu as shown in figure 2(a). In reality, the partially-grown CVD graphene on Cu foil is hardly discernible from the non-oxidized Cu [18, 19]. In figure 2(b), the graphene edge is highlighted in the DF, and the grain boundary and protruding surface of Cu are brightened by Rayleigh scattering. However, it is evident from the CLSM image of figure 2(d) that the CLSM enables very distinct and selective imaging of CVD grown graphene on Cu foil, compared to BF and DF images. In the DF image, the roughness of the Cu foil was also highlighted as indicated by the red dotted circle, but the graphene domain was clearly visible only in the CLSM. The AFM image of the CVD grown graphene on Cu foil shown in figure 2(d) was captured in the area marked with the red square in CLSM image of figure 2(c). As reported earlier, the Cu step was well observed beneath the graphene domain and the Cu roughness was relatively higher near the graphene edge, which highlights the graphene domains in DF image [8, 9]. However, no apparent height difference was observed at the interface between graphene domain and Cu.

2.2. Variable reflectance contrast upon the laser wavelength

Figures 3(a)–(d) show the CLSM images of the CVD-grown graphene on Cu foil obtained under four different laser wavelengths: 405, 488, 543, and 633 nm. Although the illuminated area is identical, the images are significantly different. It clearly displays the contrast between graphene and Cu dependent on the incident laser wavelength. The greatest contrast was obtained under the shortest wavelength of 405 nm. The grayscale histograms below CLSM images were acquired from the identical area shown as a red box in figures 3(a)–(d). They were separated with two grayscale peaks of relatively bright graphene and dark Cu, which are well fitted to red and black Gaussian distribution curve, respectively. As visibly seen in the grayscale histogram, these two peaks of graphene and Cu gradually come closer as the incident laser wavelength increases and eventually become almost indistinguishable from each other at 633 nm. The reflectance contrast of graphene on Cu, R_C, was extracted from these two Gaussian peaks of graphene and Cu in the grayscale histogram. It is computed by dividing the median of the Gaussian curve of graphene by that of Cu. The values are 1.260, 1.116. 1.057 and 1.025 at the respective wavelengths of 405, 488, 543, and 633 nm.

Then, the sample of CVD-graphene grown on Cu was illuminated with and without pinhole, and the acquired images were compared with each other (figure S2 in supplementary material). Interestingly, the CLSM images were identical regardless of the presence/absence of the pinhole at all wavelengths. This suggests that the highly visible CLSM image of CVD graphene grown on Cu foil is not a confocal image produced by a pinhole, which would only select the in-focus region and eliminate all light from the out-of-focus plane. The depth of focus for $\times 100$ objective is about 490 nm, far exceeding the graphene thickness of 0.3 nm. Therefore, all CLSM images of CVD grown graphene on Cu were taken without a pinhole in this experiment.

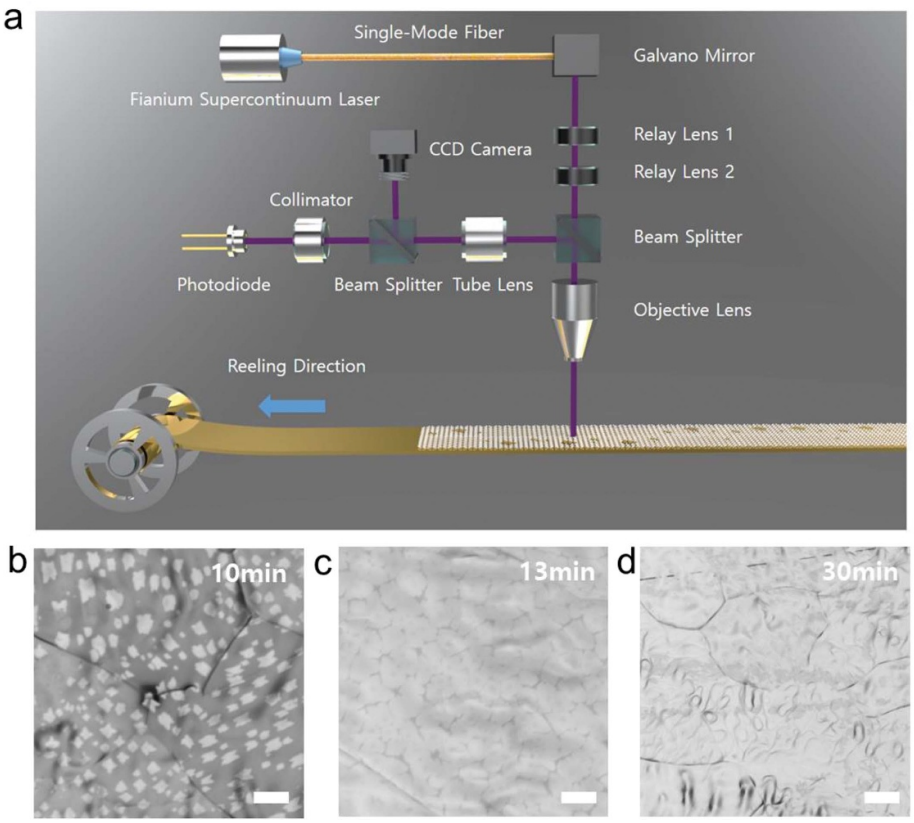

Figure 1. Concept of *in-situ* monitoring of the as-grown CVD graphene on Cu using CLSM. (a) The concept of monitoring the as-grown CVD graphene on Cu foil during the continuous roll-to-roll synthetic process using the reflective mode CLSM. (b)–(d) The CLSM images of the CVD graphene with various coverage from sub-monolayer to fully covered on Cu foil controlled by growth time of 10, 13, and 30 min, respectively. High visibility of graphene on Cu in CLSM images of (b)–(d), in which the graphene domain is a bright region and Cu is a dark region, makes it possible to determine whether graphene growth is complete. Scale bar: 10 μm.

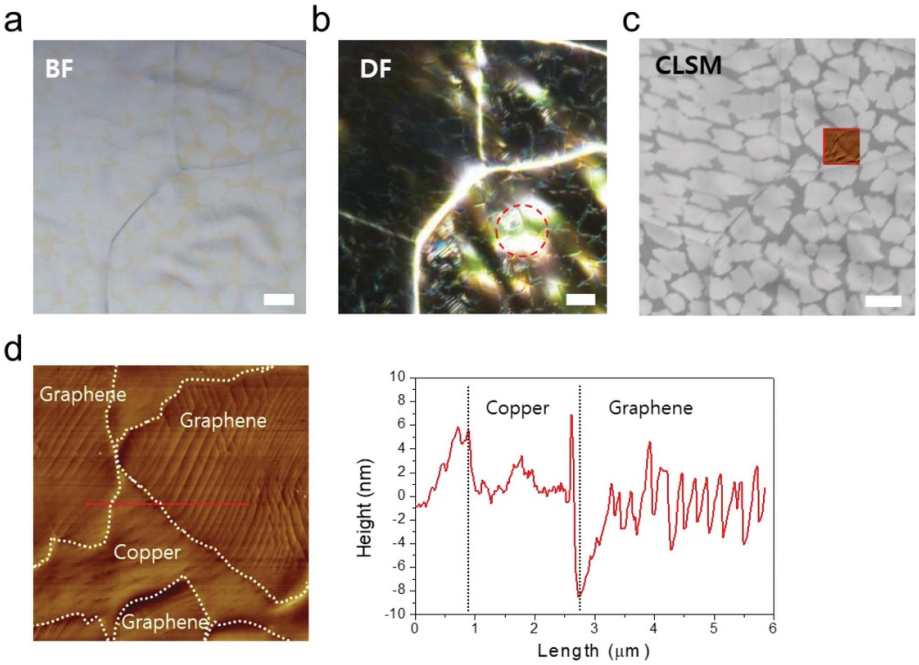

Figure 2. Comparison of BF, DF and CLSM images of CVD graphene on Cu. The images of CVD-grown graphene on Cu foil with coverage of sub-monolayer in the same region obtained by (a) bright field microscope, (b) dark field microscope, and (c) CLSM. The morphology of graphene domains on Cu foil was measured by AFM, as shown in (d). The height profile in the right, which is taken at a red dotted line in (d), clearly shows that the Cu steps beneath graphene domain, but no apparent height difference at the interface between Cu and graphene domain. Scale bar: 10 μm.

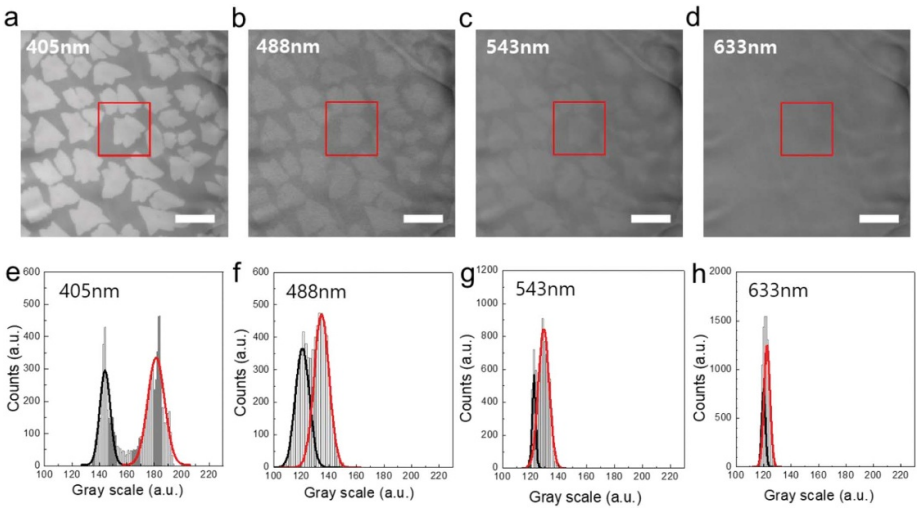

Figure 3. Dependence of CLSM images on the incident laser wavelength. The CLSM images of the CVD-grown graphene on Cu foil obtained under four different laser wavelengths of (a) 405, (b) 488, (c) 543, and (d) 633 nm, respectively. The grayscale histograms in (e) and (f) were obtained in the area indicated by the red box in each CLSM image above. The black and red Gaussian curves in the grayscale histogram correspond to dark Cu and bright graphene, respectively.

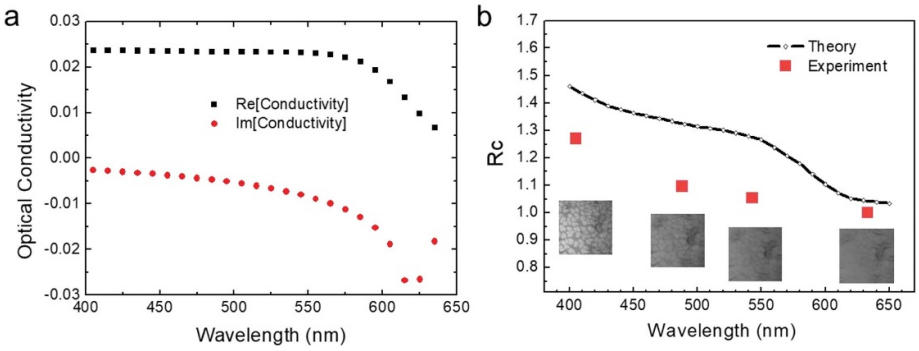

Figure 4. Measured and calculated reflectance contrast with optical conductivity. (a) The real and imaginary parts of the optical conductivity of graphene were drawn according to equations (3) and (4) as a function of wavelength. (b) The calculated and measured *Rc* of graphene on Cu were compared at four laser wavelengths of 405, 488, 543, and 633 nm, respectively.

2.3. Theory of reflectance contrast in CLSM image

Here, we investigate the origin of the high contrast seen in the CLSM of graphene grown on Cu by CVD. To calculate the optical reflectance spectra, we assumed an independent layer approximation between Cu and graphene sheets (figure S3 in supplementary material). We applied Fresnel's interference formula to calculate the optical contrast of CVD grown graphene on Cu as following

$$Rc(\omega) = \left| \frac{n_{cu}(\omega) + \frac{\sigma_{GP}(\omega)}{c\varepsilon_0} - 1}{n_{cu}(\omega) + \frac{\sigma_{GP}(\omega)}{c\varepsilon_0} + 1} \right|^2 \Big/ \left| \frac{n_{cu}(\omega) - 1}{n_{cu}(\omega) + 1} \right|^2 \quad (1)$$

where n_{Cu} is the refractive index of copper, σ_{GP} is the optical conductivity of graphene, ε_0 is the dielectric permittivity of vacuum, and c is the speed of light [16]. Here, $Rc > 1$ is judged by the CLSM images in the experiment. We set the refractive indices of Cu as $1.3009 + \mathrm{i}\,2.1595$, $1.2297 + \mathrm{i}\,2.5379$, $1.0523 + \mathrm{i}\,2.5833$, $0.26965 + \mathrm{i}\,3.4106$ for 405, 488, 543, and 633 nm, respectively. When the approximated optical conductivity of $\frac{\sigma_{GP}(\omega)}{c\varepsilon_0} \sim \pi\alpha$ is set near Dirac-cone, the optical reflectance contrast *Rc* yields unphysical values of less than 1 [20]. This indicates that the optical conductivities of graphene on Cu have different spectra in the visible range. Therefore, we applied a tight-binding model to estimate the optical properties of graphene on Cu [21–25]. Under Dirac-cone approximation, we consider up to the second-order term of the tight-binding model to account for the visible range of the spectrum. For wavelengths below 400 nm, strong carrier-carrier interaction leads to van Hove singularity in the electronic joint density of states. Therefore, our approximation applies only within the visible spectra (E < 3.1 eV) or less. If the electronic temperature value is lower than the chemical potential, i.e. $T/\mu \rightarrow 0$, the optical conductivity is Drude-like given by intraband and interband contributions [24]:

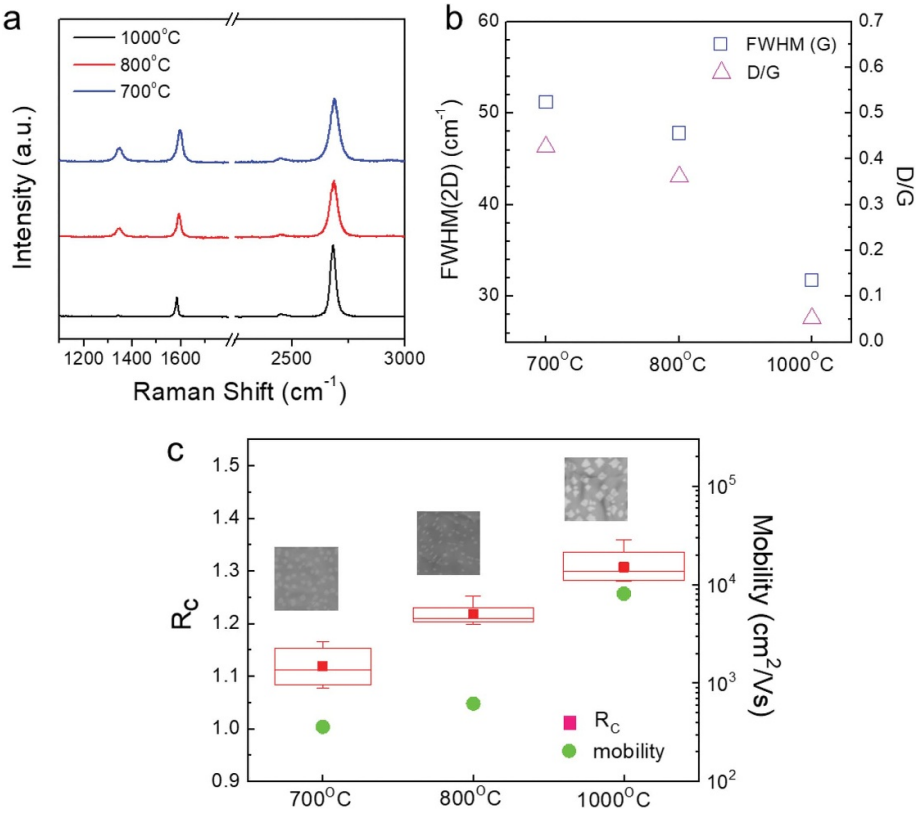

Figure 5. Raman analysis and reflectance contrast of CVD graphene grown at different temperature. (a) The Raman spectrum of CVD graphene grown on Cu foil at different temperature of 700, 800, and 1000°C, respectively. (b) The FWHM of 2D peak and the intensity ratio of D/G peak obtained from the Raman spectrum of (a) are compared with the growth temperature. (c) The carrier mobility and the statistical analysis of R_C of CVD graphene are compared with the growth temperature. The carrier mobility is calculated using the equation with FWHM of 2D peak and the *Rc* is measured from the line profile of grayscale in the CLSM images shown in the inset.

$$\sigma = \sigma_{\text{intraband}} + \sigma_{\text{interband}}$$
$$\sigma_{\text{intraband}} = i\frac{e^2\mu}{\pi\hbar^2(\omega + i\gamma)}$$
$$\sigma_{\text{interband}} = \frac{e^2}{4\hbar}\{\theta(\hbar\omega - |2\mu|)\} + i\frac{1}{\pi}\log\left|\frac{\hbar\omega + |2\mu|}{\hbar\omega - |2\mu|}\right|, \quad (2)$$

where e is the charge of an electron and $\hbar$ is Plank constant. The $\theta(\mathrm{x})$ in equation (2) is Heaviside-step function, accounting for Pauli blocking. We assume that the collision rate is negligible compared to $\gamma \ll \omega$. Temperature corrections lead to real and imaginary parts of the optical conductivities [25, 26].

$$\mathrm{Re}[\sigma] = \sigma_0\frac{\pi}{12\sqrt{3}}\frac{t^2}{\hbar\omega}\rho\left(\frac{\hbar\omega}{2}\right)\left(18 - \left(\frac{\hbar\omega}{t}\right)^2\right) \times \left[\tanh\frac{\hbar\omega + 2\mu}{4k_BT} + \tanh\frac{\hbar\omega - 2\mu}{4k_BT}\right], \quad (3)$$

$$\mathrm{Im}[\sigma] \approx \sigma_0\frac{\pi}{3\sqrt{3}}\frac{t^2}{\hbar\omega} \mathrm{Re}\left[\int_0^{3t} dE\rho(E)g\left(\frac{E}{t}\right)[f_{\mathrm{FD}}(-E) - f_{\mathrm{FD}}(E)] \times \frac{4E}{(\hbar\omega + i0^+)^2 - (2E)^2}\right], \quad (4)$$

where $\sigma_0 = e^2/4\hbar$ is termed the ac universal conductivity of the graphene, t is the hopping parameter connecting first-nearest neighbors with the value of the order 3 eV, k_B is the Boltzmann constant, $\rho(\mathrm{E})$ is the density of states per spin per unit cell, and $f_{\mathrm{FD}}(x) = 1/\left(e^{(x-\mu)/k_BT} + 1\right)$ is the Fermi–Dirac function, respectively. Here the unknown function $\mathrm{g}(\mathrm{x})$ is defined as $\mathrm{g}(\mathrm{x}) = 18 - 4x^2$. In figure 4(a), the optical conductivity calculated by the equations (3) and (4) is plotted as a function of wavelength for the range of laser wavelengths used in this experiment.

2.4. The coincidence between the calculated and measured reflectance contrast

Next, we applied the optical conductivity of equation (3) and (4) to calculate the reflectance contrast of CVD-grown graphene on Cu at laser wavelengths of 405, 488, 543, and 633 nm. The calculated contrast is 1.447, 1.326, 1.277, 1.043 at 405, 488, 543, 633 nm, respectively. The calculated *Rc* were all >1, which is consistent with the experimental results. The calculated experimental and theoretical *Rc* values are compared in figure 4(b). The wavelength dependence of the calculated *Rc* follows the same trend as the measured, suggesting that the assumption of our calculation holds true. However, the calculated and

measured *Rc* exhibit a difference of about 0.2 at all wavelengths except 633 nm at which the *Rc* is very close to 1. This difference can be attributed to the fact that CVD grown graphene has some atomic defect and tensile strain caused by the different thermal expansion coefficient of graphene and Cu, providing a lower optical conductivity than the ideal value [17, 27, 28].

In addition, we took the CLSM image of CVD graphene transferred onto Cu by the wet transfer method and compared it with that of CVD graphene grown on Cu. The *Rc* value of the CVD graphene transferred on Cu is <1 with dark graphene relative to Cu in the CLSM image (figure S4 in supplementary material). We infer that the reversed contrast in graphene transferred on Cu comes from the difference in the refractive index of Cu oxide thin film on Cu surface and the foreign matter or air gap present between the transferred graphene and Cu foil [29, 30].

2.5. Characterization of CVD graphene on Cu with CLSM

According to equation (1), it is expected that the contrast of graphene in the CLSM image varies with the optical conductivity of graphene, $\sigma_{GP}(\omega)$, which could make CLSM applicable to characterize the CVD graphene.

To further confirm this, we synthesized CVD graphene at different temperature of 700, 800, and 1000°C and their corresponding Raman spectrum are shown in figure 5(a). The full width of half maximum (FWHM) of 2D and the intensity ratio of D/G are extracted from the Raman spectrum in figure 5(a) and plotted as a function of the growth temperature in figure 5(b). It clearly shows that the FWHM of 2D and the D/G intensity ratio decrease as the growth temperature increases. It has been demonstrated in the previous study that the carrier mobility of CVD graphene is closely related to the FWHM of 2D and can be estimated by the empirical equation as a function of the FWHM of 2D [31, 32]. Following this, we calculated the carrier mobility of CVD graphene grown at 700, 800, and 1000°C from the FWHM of 2D peak, of which value is 357, 619 and 8105 cm^2/Vs at 700, 800, and 1000°C, respectively. Now, we compared the CLSM images of CVD graphene grown at different temperature. To see R_C of CVD graphene in the CLSM image, the CVD graphene was not fully grown on Cu foil by keeping the growth time for 13 min.

We analyzed the line profiles of grayscale using CLSM images for more than 10 graphene domains instead of grayscale histogram since the small-sized graphene domain produces small peaks, making it difficult to distinguish the graphene and Cu peaks in the grayscale histogram (figure S5 in supplementary material). The average resultant *Rc*, obtained by the grayscale ratio of graphene to Cu, was 1.12, 1.22 and 1.31 for CVD graphene grown at 700, 800 and 1000°C, respectively. Figure 5(c) shows that the *Rc* decreases as the growth temperature decreases, which has a same tendency with the carrier mobility of CVD graphene. Therefore, it is considered that the reduced optical conductivity of CVD graphene having a lower carrier mobility is probably responsible for lower *Rc* of CVD graphene grown at low temperature.

We also compared the CLSM images of pristine and nitrogen-doped CVD graphene by N_2 plasma treatment [33, 34]. As a result, the contrast of nitrogen-doped graphene on Cu appears to be weaker than that of pristine graphene. The *Rc* values of pristine and nitrogen-doped graphene on Cu acquired from CLSM images is 1.24 and 1.13, respectively (figure S6 in supplementary material). As discussed above, the low *Rc* of nitrogen-doped graphene is probably induced by reduced electrical and optical conductivity through nitrogen doping as reported in many previous works [35]. Based on these results, we suggest that the reflectance mode CLSM can be applied to monitor the quality as well as the growth step of CVD graphene *in-situ* during the growing process.

3. Conclusion

This study demonstrates that the reflective mode of CLSM enables real-time evaluation of CVD graphene on Cu foil by monitoring the changes of reflectance contrast, *Rc*, of graphene relative to that of Cu. In comparison to BF or DF, the graphene domain is more clearly distinguishable in the CLSM image, enabling the rapid evaluation of CVD graphene coverage on Cu foil. The *Rc* of graphene measured from the CLSM image for varying incident laser wavelength was consistent with the *Rc* calculated from the Fresnel's interference formula in which the optical conductivity of graphene is given as a function of wavelength. It was experimentally observed that nitrogen-doped and defective graphene have lower *Rc* than pristine graphene, which is due to the lower optical conductivity of defective graphene as speculated. Based on these results, we suggest CLSM as a powerful tool for *in-situ* monitoring and qualification of CVD graphene on Cu foil, which serve as a key factor to promote reliability in an industrial mass production of graphene.

4. Method

4.1. Growth and doping of CVD graphene

CVD graphene was synthesized on 25 μm thick Cu foil (99.7% in purity) through a low-pressure CVD method. A mixture of hydrogen and methane gases (H_2 5 sccm/CH_4 80 sccm) were introduced into a quartz tube furnace and heated to the desired temperature under a pressure of 30 mTorr, followed by the annealing of Cu foil under hydrogen atmosphere for

30 min. The CH_4/H_2 gas flowing time was differentiated to control the coverage of graphene layer on Cu foil from a sub-monolayer to a fully covered monolayer. To synthesize nitrogen-doped graphene, the as-grown CVD graphene on Cu foil was treated with N_2 plasma for 5 s. To generate N_2 plasma, a plasma chamber was filled with N_2 gas (5 sccm) was treated with a RF power of 10 W and evacuated to a pressure of 10^{-3} Torr.

4.2. Characterization

The CVD-grown graphene on Cu foil was characterized by an optical microscope (Olympus CX41) in BF and DF modes, atomic force microscopy (AFM), Raman spectroscopy, and x-ray photoelectron spectroscopy. The surface morphology of CVD-grown graphene on Cu was observed over $10 \times 10\ \mu m^2$ using AFM in non-contact mode with a scanning rate of 0.3 Hz (Park system, XE-100 model). The Raman measurement was carried out using Renishaw micro-Raman spectroscopy system. All samples were excited by an Ar^+ laser with an excitation power of 120 mW at a wavelength of 514 nm with a spot size of 1 μm. x-ray photoelectron spectroscopy (XPS) measurement was carried out on a Thermo Scientific Sigma Probe ESCA spectrometer using a monochromic Al x-ray source.

4.3. Confocal laser scanning microscopy

The CVD graphene on Cu foil was imaged by LSM 710 (Carl Zeiss, Germany) in reflection mode with four different visible lasers for illumination: diode ($\lambda_{diode} = 405$ nm), Ar ($\lambda_{Ar} = 488$ nm) and HeNe ($\lambda_{HeNe} = 543, 633$ nm). For a highly magnified image with an objective of x100 (N.A. = 1.30), the sample was loaded on a stage covered with a glass microscope slide down after putting oil on an objective to achieve the CLSM image with high resolution. Then, the laser was focused on the samples, and the reflected images were collected by a photomultiplier tube. The distance between the sample surface and the objective lens are adjusted to compensate for chromatically different focal distances. We operated the CLSM with the pinhole open to prevent any effect of the depth of focus and form images with the reflectance contrast. The images acquired from with and without a pinhole at different laser wavelengths are summarized in figure S2. A grayscale histogram of the acquired image was analyzed using the LSM 710 ZEN software (Carl Zeiss, Germany). Multilayer graphene films grown on Ni or Cu and h-BN on Cu were also imaged by CLSM, showing a reversed contrast or maximum contrast at longer laser wavelengths as summarized in figures S7–10.

4.4. Simulation

The optical conductivity of graphene is derived from the tight-binding approximation. The carriers in graphene can be expressed by the relativistic massless Dirac equation in (2 + 1) dimensions. The Dirac Hamiltonian $H = V_F \sigma_\alpha p_\alpha$ gives the energy spectrum of charge carriers in the electron (m = 0) and hole (m = 1) bands in $E_{\vec{k}m} = (-1)^m V_F \hbar k$. The corresponding wave function is $\left|\vec{k}m\right\rangle$. Here the σ_α's are Pauli matrices with $\alpha = (x, y)$, p_α is the momentum operator, $\vec{k} = (k_x, k_y)$, and $k = \left|\vec{k}\right|$ is the wave vector. Using Kubo formula, the effective conductivity of the graphene can be obtained consisting of intraband and interband contributions, i.e. $\sigma(\omega) = \sigma_{\text{intraband}}(\omega) + \sigma_{\text{interband}}(\omega)$, where $\sigma_{\text{intraband}}(\omega) = i\frac{e^2\mu}{\pi\hbar^2(\omega+i\gamma)}$, $\sigma_{\text{interband}}(\omega) = \frac{e^2}{4\hbar}\{\theta(\hbar\omega - |2\mu|)\} + i\frac{1}{\pi}\log\left|\frac{\hbar\omega+|2\mu|}{\hbar\omega-|2\mu|}\right|$.

If the graphene lies between medium 1 (air) and 2 (copper), the boundary conditions from Maxwell's equations at z = 0 are given by:

$$\left[\varepsilon_1\left(\vec{E}_i + \vec{E}_r\right) - \varepsilon_2\vec{E}_t\right]\cdot\vec{n} = \rho^{graphene}$$
$$\left[\vec{k}_i\times\vec{E}_i + \vec{k}_r\times\vec{E}_r - \vec{k}_t\times\vec{E}_t\right]\cdot\vec{n} = 0$$
$$\left[\vec{E}_i + \vec{E}_r - \vec{E}_t\right]\times\vec{n} = 0$$
$$\frac{1}{\omega}\left[\frac{1}{\mu_1}\left(\vec{k}_i\times\vec{E}_i + \vec{k}_r\times\vec{E}_r\right) - \frac{1}{\mu_2}\left(\vec{k}_t\times\vec{E}_t\right)\right]\times\vec{n} = \vec{j}_x = \sigma(\omega)\vec{E}_x$$

where ε_1 and ε_2 are the permittivity and μ_1 and μ_2 are the permeabilities of the two media. Here, $\rho^{graphene}$ is the graphene charge density, and $\vec{E}_i$, $\vec{E}_r$, and $\vec{E}_t$ are the incident, reflected, and transmitted electric fields. Solving further leads us to obtain:

$$(E_i - E_r)\cos\theta_1 - E_t\cos\theta_2 = 0$$
$$\sqrt{\frac{\varepsilon_1}{\mu_1}}(E_i + E_r) - \sqrt{\frac{\varepsilon_1}{\mu_1}}E_t = \sigma(\omega)E_t\cos\theta_2$$

Note that the magnetic fields are perpendicular to the plane of incidence. If we apply the continuity equation in momentum space,

$$\rho^{graphene} = \frac{k_x}{\omega}j_x(\omega) = \frac{k_x}{\omega}\sigma(\omega)E_x = \frac{k_x}{\omega}\sigma(\omega)E_t\cos\theta_2$$

With zero magnetic permeabilities, we obtain the transmission and reflection coefficients:

$$t_p \equiv \frac{E_t}{E_i} = \frac{2n_1\cos\theta_1}{n_1\cos\theta_2 + n_2\cos\theta_1 + \frac{\sigma(\omega)\cos\theta_1\cos\theta_2}{c\varepsilon_0}},$$
$$r_p \equiv \frac{E_r}{E_i} = \frac{-n_1\cos\theta_2 + n_2\cos\theta_1 + \frac{\sigma(\omega)\cos\theta_1\cos\theta_2}{c\varepsilon_0}}{n_1\cos\theta_2 + n_2\cos\theta_1 + \frac{\sigma(\omega)\cos\theta_1\cos\theta_2}{c\varepsilon_0}}.$$

Note that if graphene is absent then the above coefficients lead to the ordinary results. Finally, we get the reflectance and transmittance as a function of wavelength and chemical potential:

$$R_p = |r_p|^2$$
$$T_p = \frac{n_2\cos\theta_2}{n_1\cos\theta_1}|t_p|^2$$

Acknowledgments

This research was supported by the Basic Science Research Program through the National Research Foundation of Korea (NRF) funded by the Ministry of Education (Grant Numbers NRF-2018R1D1A1B07049592, NRF-2017R1A2B4007219), the Technology Innovation Program (or Industrial Strategic Technology Development Program (10079969, 10079974) funded By the Ministry of Trade, Industry & Energy (MOTIE, Korea), the Nano Material Technology Development Program through the National Research Foundation of Korea (NRF) funded by the Ministry of Science, ICT and Future Planning (2016M3A7B4910458) funded by the Ministry of Science, ICT, and Future Planning of Korea Government, and the Research and Business Development Program (P0009524, 2019) funded by the Korea Institute for Advancement of Technology(KIAT) and the Ministry of Trade, Industry and Energy (MOTIE).

Author contributions

B.H.H. and Y.S.W. supervised the project. Y.S.W conceived the original idea of using CLSM for a real-time quality-assessment tool. B.H.H., Y.S.W., D.J.K., and Y. S. contributed to the study design. D.J.K., Y.S., I.J., J.M., M.P., Y.S.W., and B.H.H contributed to overall data collection and interpretation. C.W.L., and H.J. contributed to simulation and analysis. D.J.K., C.W.L., Y.S., Y.S.W., and B.H.H. wrote the paper. All authors discussed and commented on the manuscript.

Conflict of interest

The authors declare no competing interests.

ORCID iDs

Dong Jin Kim https://orcid.org/0000-0003-1904-8904
Chang-Won Lee https://orcid.org/0000-0003-0546-0439
Yun Sung Woo https://orcid.org/0000-0002-4588-313X
Byung Hee Hong https://orcid.org/0000-0001-8355-8875

References

[1] Bae S *et al* 2010 Roll-to-roll production of 30-inch graphene films for transparent electrodes *Nat. Nanotechnol.* **5** 574
[2] Juang Z-Y, Wu C-Y, Lu A-Y, Su C-Y, Leou K-C, Chen F-R and Tsai C-H 2010 Graphene synthesis by chemical vapor deposition and transfer by a roll-to-roll process *Carbon* **48** 3169–74
[3] Polsen E S, McNerny D Q, Viswanath B, Pattinson S W and Hart A J 2015 High-speed roll-to-roll manufacturing of graphene using a concentric tube CVD reactor *Sci. Rep.* **5** 10257
[4] Yoon D, Moon H, Son Y-W, Choi J S, Park B H, Cha Y H, Kim Y D and Cheong H 2009 Interference effect on Raman spectrum of graphene on SiO 2/Si *Phys. Rev.* B **80** 125422
[5] Blake P, Hill E, Castro Neto A, Novoselov K, Jiang D, Yang R, Booth T J and Geim A K 2007 Making graphene visible *Appl. Phys. Lett.* **91** 063124
[6] Jung I, Pelton M, Piner R, Dikin D A, Stankovich S, Watcharotone S, Hausner M and Ruoff R S 2007 Simple approach for high-contrast optical imaging and characterization of graphene-based sheets *Nano Lett.* **7** 3569–75
[7] Wu X, Zhong G and Robertson J 2016 Nondestructive optical visualisation of graphene domains and boundaries *Nanoscale* **8** 16427–34
[8] Kong X, Ji H, Piner R D, Li H, Magnuson C W, Tan C, Ismach A, Chou H and Ruoff R S 2013 Non-destructive and rapid evaluation of chemical vapor deposition graphene by dark field optical microscopy *Appl. Phys. Lett.* **103** 043119
[9] Kang J H, Moon J, Kim D J, Kim Y, Jo I, Jeon C, Lee J and Hong B H 2016 Strain relaxation of graphene layers by Cu surface roughening *Nano Lett.* **16** 5993–8
[10] Ding D, Hibino H and Ago H 2017 Grain boundaries and gas barrier property of graphene revealed by dark-field optical microscopy *J. Phys. Chem.* C **122** 902–10
[11] Nguyen V L *et al* 2015 Seamless stitching of graphene domains on polished copper (111) foil *Adv. Mater.* **27** 1376–82
[12] Kim D W, Kim Y H, Jeong H S and Jung H-T 2012 Direct visualization of large-area graphene domains and boundaries by optical birefringency *Nat. Nanotechnol.* **7** 29
[13] Duong D L *et al* 2012 Probing graphene grain boundaries with optical microscopy *Nature* **490** 235
[14] Panchal V *et al* 2018 Confocal laser scanning microscopy for rapid optical characterization of graphene *Commun. Phys.* **1** 83
[15] Ghamsari B G *et al* 2012 Measuring the thickness of few-layer graphene by laser scanning microscopy *2012 Conf. on Precision Electromagnetic Measurements* (IEEE) pp 456–7
[16] Ivanov I G, Hassan J U, Iakimov T, Zakharov A A, Yakimova R and Janzén E 2014 Layer-number determination in graphene on SiC by reflectance mapping *Carbon* **77** 492–500
[17] Yuan S, Roldán R, De Raedt H and Katsnelson M I 2011 Optical conductivity of disordered graphene beyond the Dirac cone approximation *Phys. Rev. B* **84** 195418
[18] Chen S *et al* 2011 Oxidation resistance of graphene-coated Cu and Cu/Ni alloy *ACS Nano* **5** 1321–7
[19] Schriver M, Regan W, Gannett W J, Zaniewski A M, Crommie M F and Zettl A 2013 Graphene as a long-term metal oxidation barrier: worse than nothing *ACS Nano* **7** 5763–8
[20] Nair R R, Blake P, Grigorenko A N, Novoselov K S, Booth T J, Stauber T, Peres N M R and Geim A K 2008 Fine structure constant defines visual transparency of graphene *Science* **320** 1308–1308
[21] Colloquium: P N 2010 The transport properties of graphene: an introduction *Rev. Mod. Phys.* **82** 2673
[22] Gusynin V and Sharapov S 2006 Transport of Dirac quasiparticles in graphene: Hall and optical conductivities *Phys. Rev.* B **73** 245411
[23] Mikhailov S A and Ziegler K 2007 New electromagnetic mode in graphene *Phys. Rev. Lett.* **99** 016803
[24] Falkovsky L and Pershoguba S 2007 Optical far-infrared properties of a graphene monolayer and multilayer *Phys. Rev.* B **76** 153410
[25] Stauber T, Peres N and Geim A 2008 Optical conductivity of graphene in the visible region of the spectrum *Phys. Rev.* B **78** 085432
[26] Cheon S, Lee C W, Baik C W and Jeong H 2017 Tunable optical responses of a graphene-gold nanoparticle composite for visible light *New Phys.: Sae Mulli* **67** 684–95

[27] Deng B et al 2018 Anisotropic strain relaxation of graphene by corrugation on copper crystal surfaces Small 14 1800725
[28] Yarmohammadi M 2016 Strain effects on the optical conductivity of gapped graphene in the presence of Holstein phonons beyond the Dirac cone approximation AIP Adv. 6 085008
[29] Tahir D and Tougaard S 2012 Electronic and optical properties of Cu, CuO and Cu_2O studied by electron spectroscopy J. Phys.: Condens. Matter 24 175002
[30] Ochoa-Martínez E, Gabás M, Barrutia L, Pesquera A, Centeno A, Palanco S, Zurutuza A and Algora C 2015 Determination of a refractive index and an extinction coefficient of standard production of CVD-graphene Nanoscale 7 1491–500
[31] Robinson J A et al 2009 Correlating Raman spectral signatures with carrier mobility in epitaxial graphene: a guide to achieving high mobility on the wafer scale Nano Lett. 9 2873–6
[32] Woo Y S, Lee D W and Kim U J 2018 General Raman-based method for evaluating the carrier mobilities of chemical vapor deposited graphene Carbon 132 263–70
[33] Rybin M, Pereyaslavtsev A, Vasilieva T, Myasnikov V, Sokolov I, Pavlova A, Obraztsova E, Khomich A, Ralchenko V and Obraztsova E 2016 Efficient nitrogen doping of graphene by plasma treatment Carbon 96 196–202
[34] Wang C et al 2012 Plasma-assisted growth and nitrogen doping of graphene films Appl. Phys. Lett. 100 253107
[35] Yanilmaz A, Tomak A, Akbali B, Bacaksiz C, Ozceri E, Ari O, Senger R T, Selamet Y and Zareie H 2017 Nitrogen doping for facile and effective modification of graphene surfaces RSC Adv. 7 28383–92